Semnan University

Progress in Physics of Applied Materials

journal homepage: https://ppam.semnan.ac.ir/

Investigating the Influence of Single Fe and Two Fe co-doping on the Structural and Magnetic Properties of Monolayer Pt_2Te_4 Pentagonal: A First Principle Study

Mojtaba Gholami

Department of Physics, Payame Noor University, Tehran, Iran

ARTICLE INFO

Article history:
Received: 8 May 2024
Revised: 22 July 2024
Accepted: 3 August 2024

Keywords:
co-doping
Pt_2Te_4 Pentagonal
Magnetic moments
Ferromagnetic coupling

ABSTRACT

The manipulation of magnetic characteristics in 2D materials is essential for their utilization in spintronic and magnetic devices. this study was carried out to investigate the doping process involving a single Fe dopant and the co-doping of two Fe impurities at the Pt site within the Pt_2Te_4 monolayer. The examination revealed that the introduction of a single iron (Fe) atom and a pair of Fe atoms into the non-magnetic semiconductor monolayer of Pt_2Te_4 leads to magnetic moments measuring 2 μ_B and 4μ_B, respectively. The origin of magnetic moments is observed predominantly around Fe-3d orbitals. In the instances of co-doping involving Fe-Fe substitution, four distinct configurations were examined. One of the configurations, specifically FeFe (1), was identified as the most stable due to its minimal energy level. This configuration also demonstrates a ferromagnetic coupling mechanism between the two Fe substitutions, a phenomenon that can be justified by the significant magnetic moment of 4μ_B.

1. Introduction

The identification of graphene represents a significant revolution in the exploration of different two-dimensional materials and the expansion of their applications across various physical fields such as spintronic, optoelectronics, and optical devices [1-9]. In contrast to graphene, which is composed of carbon atoms arranged in honeycomb structures, a variety of two-dimensional materials are constructed using pentagonal rings of heterogeneous atoms that include transition metals (TM) and termination groups from the periodic table [10-16]. Pentagonal monolayers are primarily composed of transition metals (TM) such as Ni, Pd, and Pt, along with nonmetals from group 6 (X) like O, S, Se, and Te. These materials are typically represented by chemical formulas such as TMX_2 and TM_2X_4 [17-22]. The arrangements derived from the two typically exhibit identical geometric patterns, with each pentagonal ring comprising of two transition metals (TM) and three chalcogen nonmetals (X). The distinguishing characteristics of the two groups are primarily attributed to the band gap values and dissimilar point groups. As an example, monolayer PdS_2 exhibits a band gap of 1.2 eV and is classified under the point group p2-1/c, while monolayer Pd_2S_4 displays a band gap of 1.12 eV and belongs to the point group p2-1/b11 [21,22]. the modulating of the magnetic properties of two-dimensional materials is considered a crucial point in the spintronic devices application. Consequently, the introduction of a doping mechanism is regarded as exceedingly effective and feasible approach for inducing changes in magnetic properties substitutional doping of 3d transition metals that has recently attracted tremendous attention, and the following refers to the results of some studies. 3d TM doping at the Pd site for the Pd_2S_4 monolayer shows that the maximum quantity of observed magnetic moments (around 3.2μB) is related to the Mn atom, and Sc and Ti impurities cannot induce magnetic moments in the system [22]. Recent research has shown that the introduction of Cr, Mn, and Fe doping into the $SnSe_2$ system leads to notable magnetization values of 3.40 μ_B, 4

* Corresponding author.
E-mail address: m_gholami@pnu.ac.ir

Cite this article as:
Gholami, M., 2024. Investigating the Influence of Single Fe and Two Fe co-doping on the Structure and Magnetic Properties of Monolayer Pt_2Te_4 Pentagonal: A First Principle Study. *Progress in Physics of Applied Materials*, *4*(2), pp.153-159.DOI: 10.22075/ppam.2024.34081.1099

μ_B, and 3.40μ_B, respectively [23]. The study conducted by Zhang demonstrate that the non-magnetic semiconductor penta-ZnO_2 exhibits magnetic properties (1.93 μ_B, 2.96μ_B) in the presence of Fe and Co atoms [24]. As resulting of doping transition metals (Mn, Fe, Co, and Ni), the WS_2 monolayer acquires magnetic moments of 1 μ_B, 2 μ_B, 3 μ_B, and 4 μ_B. Furthermore, this doping induces the manifestation of half-metallic properties in the system [25]. One method utilized in scientific research to generate magnetism involves the co-doping technique, where multiple atoms are replaced within the monolayers. The adding of two TM atoms on a ZrS_2 monolayer has resulted in the observation of total magnetic moments measuring 1, 0.98, and 1.80 μB. The magnitudes of these magnetization values are dependent on the precise positioning of impurity atoms within the ZrS_2 monolayer [26]. Five distinct arrangements were examined to investigate the substitutional co-doping of Mn and Mo atoms in the $SnSe_2$ monolayer, resulting in the achievement of total magnetic moment of 6μ_B [27]. In this study, we investigate the magnetic and electronic characteristics of a monolayer of pentagonal Pt_2Te_4 in presence of single and paired Fe dopant. The amount of magnetic moment due to doping of single and pair Fe impurities was observed to be 2μ_B and 4μ_B, respectively, which originate from electrons of the Fe-3d orbital. Four different configurations have been considered for the two Fe atoms deployment, and the most stable state has been determined by evaluating ferromagnetic (FM) and antifomagnetic (AFM) energies. According to the calculations conducted, it was observed that two iron atoms exhibit a propensity towards a ferromagnetic alignment within the system. Prior to this study, no similar research has been published in the scientific articles and the co-doping technique of two 3 atoms on pentagonal monolayers has been examined for the first time.

2. Model and calculation methods

The Orthorhombic crystal structure of the Pt_2Te_4 monolayer is examined, comprising 18 platinum atoms and 36 telluride atoms. This structure was generated by enlarging the primitive cell to a 4×4 supercell, as illustrated in Figure 1. The analysis of the single Pt_2Te_4 layer was conducted through calculations utilizing the Siesta simulation code, which based on spin-polarized density functional theory [28]. In order to inhibit the interaction between adjacent layers, a vacuum thickness of 20 angstroms (20Å) is utilized. The plane wave cut-off energy is established at 200 eV and Monkhorst-Pack with a 7 × 7 × 1 k-point configuration is employed within the first Brillouin zone. The structures endure geometric optimization procedures until the total force acting on each ion is reduced to below 0.01 eV/Å, with an energy tolerance of 10^{-5} eV set for electronic relaxation.

3. Results and discussion

The Pt_2Te_4 monolayer is a kind of 2D nonmagnetic semiconductor from the orthorhombic group, resembling the pentagonal Pd_2S_4 and Pt_2Se_4 monolayers. In this material, each Pt atom forms covalent bonds with four Te atoms, as illustrated in Figure 1(a, b). The determined indirect band gap value is around 1.38 eV, which is in agreement with findings from previous theoretical calculations [29, 30]. Based on Figure 1(a), it is evident that both the spin-up and spin-down channels within the polarization band structure exhibit symmetrical characteristics, suggesting the non-magnetic nature of the pristine Pt_2Te_4 system. now, an examination will be conducted on the structural, electronic, and magnetic characteristics, with the presence of introducing one Fe dopant (at a concentration of 0.018%) and two Fe co-dopants (at a concentration of 0.036%). The negligible values of doping concentrations indicate that the original structure configuration experience limited alteration and largely persist in a diluted state. Consequently, this enhances the reliability of analyzing the effects of doping mechanism. To simply investigate the mechanism of doping, the analysis is divided into two sections focusing on single Fe doping and two Fe-Fe co-doping, with each part being examined independently.

3.1. configuration of singly Fe-doped Pt_2Te_4

Fig. 2(a) shows the substitution scheme of one Fe atom at the site of the Pt atom. The asymmetry observed in the spin-up and spin-down channels within the band structure depicted in Figure 2(b) and the density of states (DOS) illustrated in Figure 2(c) imply that doping Fe induces magnetic properties. Despite the emergence of extra impurity states caused by spin-down near the Fermi level, the Fermi level has not been interrupted, and the system maintains its semiconducting property. Figure 2(d, e, f) illustrates the density of states (DOS) for the Fe-3d orbital, along with the DOS for the six nearest Te-4p orbitals and the four Pt-5d orbitals surrounding the Fe atom. It is observed that impurities formed confined the band gap predominantly originate from mention orbitals.

As demonstrated by the highlighted yellow rectangle inside Figure 2, the introduction of iron (Fe) doping results in a total magnetic moment of 2μ_B for the single-layer Pt_2Te_4 structure. According to the data presented in Figure 2(d, e, f, g), it can be seen that the predominant contribution to the total magnetic moment originates from the Fe-3d orbital, with a value of 2.2μ_B. It is worth noting that Te-4p and Pt-5d orbitals adjacent to Fe impurity, by producing magnetization values of -0.16μ_B and -0.012μ_B, play a magnetically insignificant role. Spin density of Figure 2(a) also confirms the extremely spin-up polarization of Fe atom, while it is not observable for Te and Pt atoms. Depending on the polarity of the local magnetic moment present on the atoms, the Fe-3d orbitals hybridize with Te-4p and Pt-5d orbitals through antiferromagnetic (AFM) coupling. In order to precisely survey magnetism origin, we further explore the role of Fe-3d orbitals. Following doping Fe at Pt atom, Fe ($3d^6$ $4s^2$) transfer four electrons to four neighboring Te atoms as the result of electronegativity deference. Thus, the orbital of Fe atom forms as Fe^{+4}($3d^4$ $4s^0$) configuration. In simple terms, the existence of the last four electrons in the Fe-3d orbital significantly influences the development of the magnetic moment. By simply observing Figure 3, it can be asserted that the spin-up states of the d_{yz}, dz^2, and d_{zx} orbitals has fully been occupied.

Furthermore, it is probable that the fourth electron has occupied the dz^2 orbital with spin-down. Consequently, the

net magnetization generated by three spin-up and one spin-down electron justify the calculated magnetic moment of 2μ_B for the Fe-doped system.

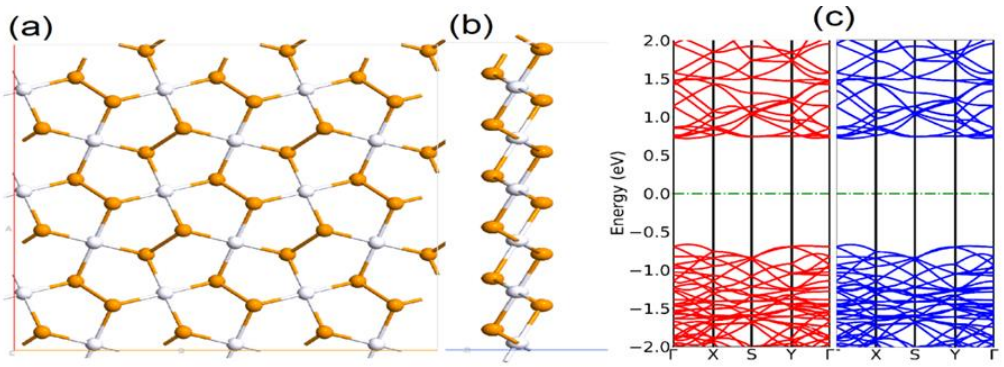

Fig. 1. (a) Top and (b) side views for the atomic structure Monolayer Pt_2Te_4 Pentagonal. The white and gray balls represent the Pt and Te atoms, respectively. (c) Band structures of the defective of Pt_2Te_4 monolayer. The red lines represent the spin-up, the blue lines represent spin-down components, and the Fermi level is indicated by dotted line.

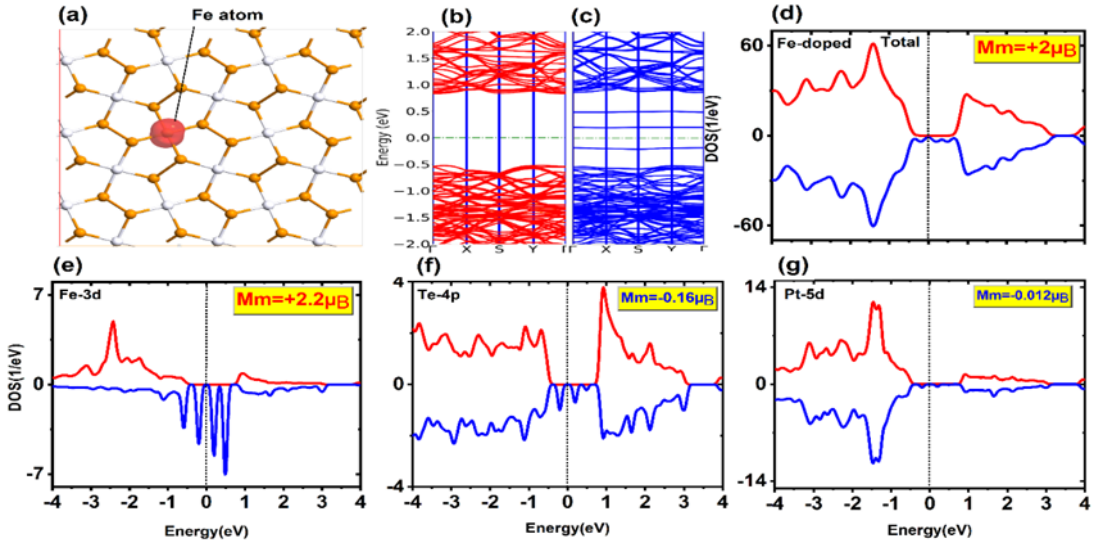

Fig. 2. (a) The spin density. (b-c) Band structures. (d) total density of state (TDOS). the density of state (DOS) of (e) Fe-3d orbital, (f) Te-4p orbital and (g) Pt-5d orbital.

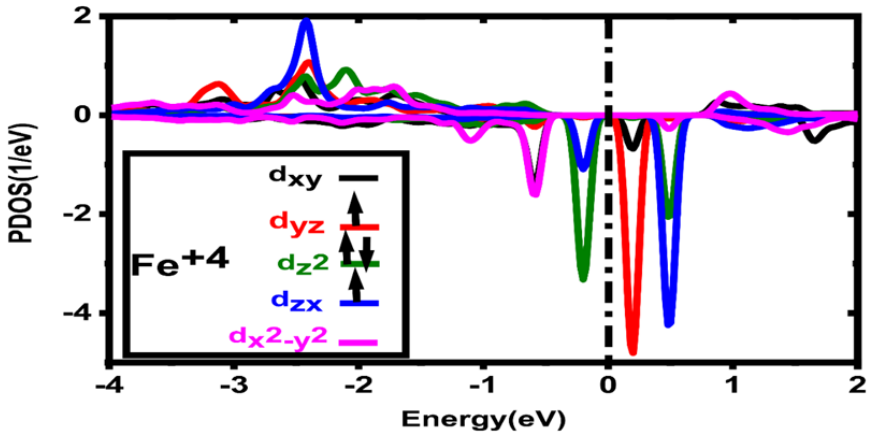

Fig.3. The partial density of states (PDOS) corresponding to the Fe-3d orbitals.

3.2. configuration of pair Fe co-doped Pt_2Te_4

In this section, we explore the impact of dual Fe impurity doping on the electronic and magnetic moments of Fe-doped Pt_2Te_4 and with results of previous section (see section 3.1) that focused on the consequences of single Fe atom doping has been compared. Based on the varying distances between two Pt atoms as depicted in Figure 4(a-d), four distinct configurations may be identified for the placement of two Fe atoms in the co-doping process. One method for recognizing the most favorable structure energetically involve computing the energy differential between ferromagnetic (FME) and antiferromagnetic (AFME) states across four distinct systems. Given the formation energies' negative values, the system's ferromagnetic nature increases as the ratio ΔE(meV)= EAFM- EFM>0 becomes larger. As can be seen from Figure 4(e), it is clear that the energy value amounts to 178 (meV) for the FeFe(1) configuration, which reveal the highest degree of stability in terms of ferromagnetism (FM) among four structures.

On the other hand, it is in good agreement with the obtained results associated with the spin density in Figure 5(c). Hence, schematic of the co-doping of two Fe atoms consistent with Figure 4(a), represents possible and reasonable choice for our examination. Furthermore, the formation energy ($E_{FeFe(i=1,2,3,4}$) for each Fe co-doped system has been calculated in comparison to the formation energy ($E_{FeFe(4)}$) as outlined below:

$$\Delta E(meV)=E_{FeFe(4)}-E_{FeFe(i=1,2,3,4)} \quad (1)$$

Hence, the FeFe(1) configuration demonstrate the greatest stability when ΔE reaches its maximum value, while the FeFe(4) state is considered the least stable when ΔE is equal to zero.

Given that the system's most stable configuration, FeFe(1), has been found as the prevalent occurrence among the various distances, an analysis of its structural, electronic and magnetic characteristics can now be conducted. The locations of impurity atoms for doping are denoted as Fe1 and Fe2 in Figure 5(a). Furthermore, the distinct geometric positions of the neighboring Te and Pt atoms surrounding the two Fe atoms are denoted by varying indices. The group of atoms Te1, Te2, and Te3 is named as the first neighboring atoms of the Fe1 atom, whereas T4, T5, and T6 are labled as the first neighbors of the Fe2 atom. The Te0 atom has an identical distance in relation to the Fe1 and Fe2 atoms. As can be noticed on Figure 5(a), the closet neighboring Pt atoms near Fe1 and Fe2 impurities denoted as (Pt1, Pt2, Pt3) and (Pt4, Pt5, Pt6) respectively.

The band structure analysis showed in Figure 4(b-c) and 5(b-c) illustrates that the introduction of Fe-Fe co-doping results in greater number of states compared to the case of single Fe doping. These impurities are exclusively derived from spin-down channels, with no evidence of spin-up effects detected within the band gap. Similar to the previous section, here the band gap value has also reduced, however, the semiconductor characteristics persist in the Fe-Fe co-doped Pt_2Te_4 monolayer. The spin density plot represented in Figure 5(d) clearly highlight the Impressive magnetization concentration on two Fe atoms within the doped system, while no neighboring atoms exhibit polarization. The DOS of the total magnetic moment and its value are exhibited in Figure 5(e), where total magnetic moment $4\mu_B$ represents the existence of the strong ferromagnetic coupling between two Fe atoms.

The magnetic moment originating from Fe1 and Fe2 atoms is lonely attributed to the Fe1-3d and Fe2-3d orbitals, with calculated values of 2.17 μ_B and 2.15 μ_B, as illustrated in Figure 5(f). From Figure 5(f), it can be observed that the predominant states within the energy range of approximately -1.5 to -3 eV are those associated with spin-up. These states are considered as the primary magnetic source for the doped Pt_2Te_4 system. Based on the magnetization measurements of -0.14μB and -0.15μB for the (Te1, Te2, Te3)-4p and (Te4, Te5, Te6)-4p orbitals, as illustrated in Figure 5(g), it can be inferred that the (Te1, Te2, Te3) and (Te4, Te5, Te6) systems through antiferromagnetic coupling with Fe1 and Fe2 impurities has been hybrid. But Te0 atom owing $+0.12\mu_B$ under the common influence of two impurities receive different magnetization distributions compared with other Te atoms, leading to the ferromagnetic coupling formation with Fe1 and Fe2 metals (see Fig.5(h)). Finally, there are the nearest Pt atoms which observed around two Fe impurities. As depicted in Figure 5(i), these atoms rarely polarized resulting in not induceing a significant amount of magnetization in the system. The downward spin direction results in the establishment of antiferromagnetic coupling with the spin of two Fe atoms.

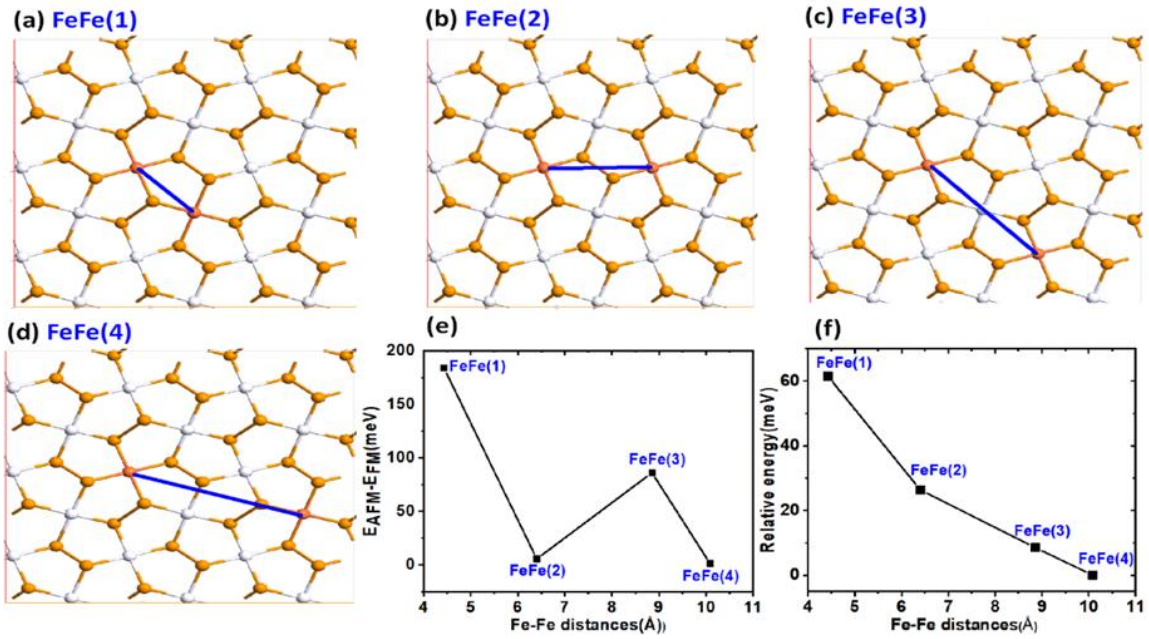

Fig. 4. (a-d) Four different configurations corresponding to the Fe-Fe doping sites. (e) Schematics of energy difference, AFM and FM, for four states. (f) Stability energy diagram for four different systems.

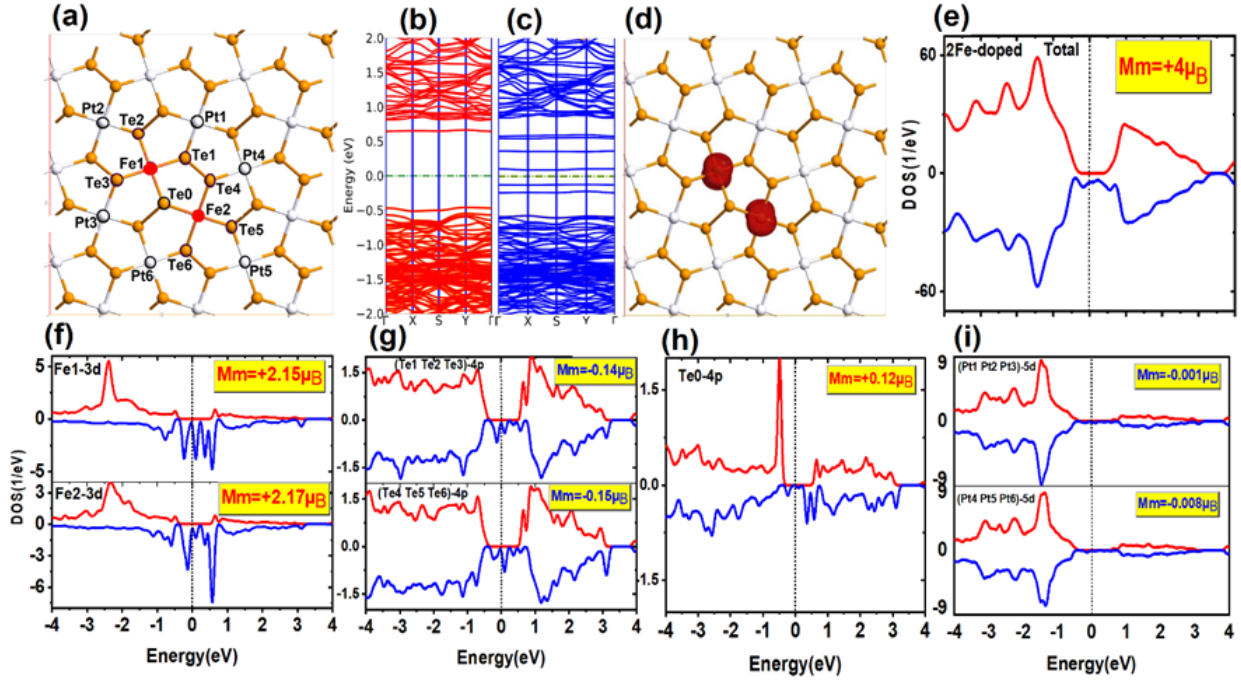

Fig. 5. (a) Top views of two Fe-doped atoms on monolayer Pt_2Te_4 at the site of two Pt atoms, also the nearest-neighboring of Pt and Te atoms. (b-c) The band structure. (d) The spin density. (e) total density of state (TDOS).) the density of state (DOS) of (f Fe-3d orbital,(g) Te-4p orbitals, (h) Te-4p orbital (bonded to two Fe atoms), (i) Pt-5d orbital.

4. Conclusion

The research was conducted to explore the doping approach involving a lone Fe dopant and the co-doping of two Fe impurities at the Pt site within the Pt_2Te_4 monolayer. The investigation demonstrated that introducing a single Fe atom and a pair of Fe atoms into the non-magnetic semiconductor Pt_2Te_4 monolayer results in the induction of magnetic moments measuring 2 μ_B and 4μ_B, respectively. The origin of magnetic moments is observed predominantly around Fe-3d orbitals. The research explored four distinct configurations for instances of substitution doping of two Fe atoms. Among these, the FeFe(1) configuration was identified as the most stable due to its minimum energy state. This configuration also displays a ferromagnetic coupling mechanism between the two Fe atoms, which is confirmed by the significant magnetic moment of 4μ_B. These findings hold promise for diverse applications in the fields of spintronics and optoelectronics.

Acknowledgements

This research received no external funding.

Conflicts of Interest

The author declares that there is no conflict of interest regarding the publication of this article.

References

[1] Song, B., Chen, X.L., Han, J.C., Wang, G., Bao, H.Q., Duan, L.B., Zhu, K.X., Li, H., Zhang, Z.H., Wang, W.Y. and Wang, W.J., 2011. Raman scattering and magnetizations studies of (Al, Cr)-codoped 4H-SiC. *Journal of magnetism and magnetic materials, 323*(22), pp.2876-2882.

[2] Mallik, S.K., Jena, A.K., Sharma, N.K., Sahoo, S., Sahu, M.C., Gupta, S.K., Ahuja, R. and Sahoo, S., 2022. Transition metal substituted MoS_2/WS_2 van der Waals heterostructure for realization of dilute magnetic semiconductors. *Journal of Magnetism and Magnetic Materials, 560*, p.169567.

[3] Gholami, M., Nazari, A., Azarin, K., Yazdanimeher, S. and Sadeghniya, B., 2013. Determination of the thickness and optical constants of metal oxide thin films by different methods. *J. Basic Appl. Sci. Res, 3*(5), pp.597-600.

[4] Jafari, A., Ghoranneviss, M., Gholami, M. and Mostahsan, N., 2015. The role of deposition temperature and catalyst thickness in graphene domains on Cu. *International Nano Letters, 5*, pp.199-204.

[5] Jafari, A., Ghoranneviss, M., Gholami, M., Salar Elahi, A. and Kavosi ghafi, A., 2016. The effects of percent and position of nitrogen atoms on electronic and thermoelectric properties of graphene nanoribbons. *Journal of Inorganic and Organometallic Polymers and Materials, 26*, pp.1095-1100.

[6] Hajakbari, F., Hojabri, A., Gholami, M. and Ghoranneviss, M., 2009. Calculation of Cu_2O thin film optical constants using the transmittance data. ISPC Proceedings, Bochum.

[7] Gholami, M., Ebrahimi Sarai, M. and Hassanpour, M., 2022. Tunable magnetic induction of 1T-$NiTe_2$ monolayer via V, Cr, Mn and Fe Transition metals atomic doping. *Quarterly Journal of Optoelectronic, 4*(2), pp.65-72.

[8] Feng, N., Mi, W., Cheng, Y., Guo, Z., Schwingenschlögl, U. and Bai, H., 2014. First principles prediction of the magnetic properties of Fe-X 6 (X= S, C, N, O, F) doped monolayer MoS_2. *Scientific reports, 4*(1), p.3987.

[9] He, J., Zhou, P., Jiao, N., Ma, S.Y., Zhang, K.W., Wang, R.Z. and Sun, L.Z., 2014. Magnetic Exchange Coupling and Anisotropy of 3 d Transition Metal Nanowires on Graphyne. *Scientific reports, 4*(1), p.4014.

[10] Jena, A.K., Mallik, S.K., Sahu, M.C., Sahoo, S., Sahoo, A.K., Sharma, N.K., Mohanty, J., Gupta, S.K., Ahuja, R. and Sahoo, S., 2022. Strain-mediated ferromagnetism and low-field magnetic reversal in Co doped monolayer WS_2. *Scientific reports, 12*(1), p.2593.

[11] Zhang, H., Zhang, Z., Zhan, Q., Liu, D., Zhao, P. and Cheng, Y., 2022. Recent advances of substitutionally doped tin dichalcogenides. *Journal of Materials Chemistry C, 10*(20), pp.7771-7782.

[12] Wang, Y., Dong, S. and Yao, X., 2023. Frustration-induced magnetic bimerons in transition metal halide CoX_2 (X= Cl, Br) monolayers. *Physica E: Low-dimensional Systems and Nanostructures, 153*, p.115776.

[13] Xue, R., Han, R., Lin, X. and Wu, P., 2023. First-principles investigate on the electronic structure and magnetic properties of 3d transition metal doped honeycomb InS monolayer. *Applied Surface Science, 608*, p.155240.

[14] Oyedele, A.D., Yang, S., Liang, L., Puretzky, A.A., Wang, K., Zhang, J., Yu, P., Pudasaini, P.R., Ghosh, A.W., Liu, Z. and Rouleau, C.M., 2017. $PdSe_2$: pentagonal two-dimensional layers with high air stability for electronics. *Journal of the American Chemical Society, 139*(40), pp.14090-14097.

[15] Ao, K.L., Shao, Y., Chan, I.N., Shi, X., Kawazoe, Y., Yang, M., Ng, K.W. and Pan, H., 2020. Design of novel pentagonal 2D transitional-metal sulphide monolayers for hydrogen evolution reaction. *International Journal of Hydrogen Energy, 45*(32), pp.16201-16209.

[16] Qu, Y., Kwok, C.T., Shao, Y., Shi, X., Kawazoe, Y. and Pan, H., 2021. Pentagonal transition-metal (group X) chalcogenide monolayers: Intrinsic semiconductors for photocatalysis. *International Journal of Hydrogen Energy, 46*(14), pp.9371-9379.

[17] Guo, Y., Zhou, J., Xie, H., Chen, Y. and Wang, Q., 2022. Screening transition metal-based polar pentagonal monolayers with large piezoelectricity and shift current. *npj Computational Materials, 8*(1), p.40.

[18] Zhao, K., Guo, Y., Shen, Y., Wang, Q., Kawazoe, Y. and Jena, P., 2020. Penta-BCN: A new ternary pentagonal monolayer with intrinsic piezoelectricity. *The journal of physical chemistry letters, 11*(9), pp.3501-3506.

[19] Liang, Q., Chen, Z., Zhang, Q. and Wee, A.T.S., 2022. Pentagonal 2D transition metal dichalcogenides: $PdSe_2$ and beyond. *Advanced Functional Materials, 32*(38), p.2203555.

[20] Wang, C.T. and Du, S., 2020. A unique pentagonal ntwork structure of the NiS_2 monolayer with high stability and a tunable bandgap. *Physical Chemistry Chemical Physics, 22*(14), pp.7483-7488.

[21] Gholami, M., Golsanamlou, Z. and Rahimpour Soleimani, H., 2022. Effects of 3d transition metal impurities and vacancy defects on electronic and magnetic properties of pentagonal Pd_2S_4: competition between exchange splitting and crystal fields. *Scientific Reports, 12*(1) p.10838.

[22] Gholami, M. and Rahimpour Soleimani, H., 2022. Magnetic and electronic properties of Pd_2S_4 monolayer dichalcogenide under doping of atoms adjacent to sulfur atom. *Quarterly Journal of Optoelectronic, 4*(1), pp.105-111.

[23] Lin, L., Pang, D., Shi, P., Su, L., Chen, Z. and Zhang, Z., 2022. First-principles calculations of magnetic and optical properties of (Mn, Mo) co-doped $SnSe_2$. *Physica Scripta, 97*(8), p.085809.

[24] Zhang, H., Wang, N., Wang, S. and Zhang, Y., 2020. Effect of doping 3d transition metal (Fe, Co, and Ni) on the electronic, magnetic and optical properties of pentagonal ZnO_2 monolayer. *Physica E: Low-dimensional Systems and Nanostructures, 117*, p.113806.

[25] Xie, L.Y. and Zhang, J.M., 2016. Electronic structures and magnetic properties of the transition-metal atoms (Mn, Fe, Co and Ni) doped WS_2: a first-principles study. *Superlattices and Microstructures, 98*, pp.148-157.

[26] Zhao, X., Chen, P., Yang, C., Zhang, X. and Wei, S., 2018. Electronic and magnetic properties of the N monodoping and (Mn, N)-codoped ZrS_2. *Journal of materials science, 53*, pp.7466-7474.

[27] Lin, L., Pang, D., Shi, P., Su, L., Chen, Z. and Zhang, Z., 2022. First-principles calculations of magnetic and optical properties of (Mn, Mo) co-doped $SnSe_2$. *Physica Scripta, 97*(8), p.085809.

[28] Soler, J.M., Artacho, E., Gale, J.D., García, A., Junquera, J., Ordejón, P. and Sánchez-Portal, D., 2002. The SIESTA method for ab initio order-N materials simulation. *Journal of Physics: Condensed Matter, 14*(11), p.2745.

[29] Ge, X., Zhou, X., Sun, D. and Chen, X., 2023. First-Principles Study of Structural and Electronic Properties of Monolayer PtX_2 and Janus PtXY (X, Y= S, Se, and Te) via Strain Engineering. *ACS omega, 8*(6), pp.5715-5721.

[30] Han, L., Zou, Y., Zeng, Q., Guan, X., Jia, B., Gao, Y., Liu, G. and Wu, L., 2022. Strong interlayer interaction in two-dimensional layered $PtTe_2$. *Journal of Solid State Chemistry, 305*, p.122657.